Journal of Basrah Researches (Sciences) **50**(2), 99 (2024)
DOI: https://doi.org/10.56714/bjrs.50.2.9

Novel Insights into the optical Properties of Poly (3-Hexylthiophene-co-Thiophene) with Varying Monomer Percentages

Ahmed Ismael [1,*], **Hussein F. Hussein** [1], **Salah S. Al-luaibi** [2]

[1] Physics Department, College of Education for Pure Sciences, Basrah University, Basrah, Iraq.
[2] Chemistry department, College of Science, Basrah University, Basrah, Iraq.

ARTICLE INFO

Received 10 May 2024
Revised 8 August 2024
Accepted 15 August 2024
Published 31 December 2024

Keywords:

Poly 3-hexylthiophene, Poly Thiophene, Copolymerization, Structure-Property Relationships, Optical Properties.

Citation: A. Ismael et al., J. Basrah Res. (Sci.) **50**(2), 99 (2024).
DOI:https://doi.org/10.56714/bjrs.50.2.9

ABSTRACT

The study explains the effect of the copolymer overlay ratio on optical properties that can be utilized in solar cell applications. Copolymers prepared by additive polymerization were characterized. The X-ray examination results characterized the samples and showed that the prepared samples of pure and composite polymers possess a high degree of crystallinity. The prepared samples were also characterized by FT-IR spectroscopy, which showed that these films had clear active groups. The optical properties of all prepared films were also studied, such as absorbance within the spectrum range (200 - 800 nm) as a function of wavelength, and Band gab Energy Eg, Excitation Energy Eo, Dispersion Energy Ed, Refractive index (no) 2, Dielectric constant at high frequencies E∞, Moments of The Optical Spectra for Crystal M-1 M-3, The Average Oscillator So, Third-order visual effect X^3. The study showed that the absorbance spectrum of the films of the materials under study is within the visible spectrum region, where the most significant peak was recorded for the pure and composite polymers at the wavelength of 485 - 495 nm. The study showed that the optical energy gap of P3HT polymer (2.78 eV) and for Thiophene (2.3 eV) and the value of the gap decreased with the doping rate increased until it reached (1.88 eV) at the copolymer rate of 70 % P3HT 30% thiophene. It showed varying thicknesses ranging from approximately 49.1 to 10.2 nanometers, and the recorded roughness of the polymer surfaces ranged from 20.7 to 5.19 nanometers.

1. Introduction

In recent years, polymer composite devices have received considerable attention owing to their remarkable optoelectronic, electrical, and magnetic properties, which open a great potential in

applications as light emitting diodes (LEDs) [1], [2], photovoltaic cells (PV) [3], [4], sensors [5], [6], photo detectors [7], [8] and transistors [9], [10], [11]. Currently, many studies have been conducted to investigate the influence of incorporation into polymer matrix on the charge transfer process, such as charge trapping and de-trapping [12], [13] and the formation of conductive filament

*Corresponding author email : ahmed.nano86@gmail.com

N: 1817-2695 (Print); 2411-524X (Online)
ine at: https://jou.jobrs.edu.iq

paths [14], [15]. There have been significant efforts to develop the optical properties of samples to enable their use in solar cells And other applications [16]. Poly(3-hexylthiophene) (P3HT) and pure thiophene materials have been extensively studied, as well as the polymeric overlay ratio (10:90, 30:70, 50:50) , because they have high solubility in organic solvents and crystallization , whose size and shape can be controlled. There are two methods for preparing polymers: addition polymerization and condensation polymerization [17]. The samples were prepared using the additive polymerization method. Poly (3-hexylthiophene) (P3HT) materials have been significantly studied for their uses in organic optoelectronics. This is because it has of their high solubility in organic solvents and controllable crystallinity [18]. Many researchers have reported tandem and hybrid structures with increased efficiency in absorbing sunlight in a wide spectral range [19]. Through the energy band gap, the optical properties of inorganic and organic nanostructures, such as photoluminescence and absorption efficiency, can be controlled through their shape, size, and properties Crystal [20].Various synthetic, processing, and hybridization methods have been studied with different nanomaterials as a means of tuning the optical properties of polymeric nanostructures [21]. To modify the optical properties, copolymers from (Poly 3-hexylthiophene) and (Thiophene) were heat-treated in an aqueous suspension, i.e., compressed in a chamber at varying temperatures [22]. After heat treatment, depending on different temperatures, the ultraviolet and visible (UV/Vis) absorption spectra changed significantly with the intensity and width of the features [23].

2. Materials

In this study, various materials were used as provided by suppliers. The monomer 3-hexylthiophene, essential for light absorption, was obtained from Meryer (SHANGHAI) CHEMICAL TECHNOLOGY CO., LTD purity. Thiophene, known for its electron-donating properties and high charge mobility, was sourced from ORGANICS USA with over 99% purity. Indium tin oxide (ITO), used for its transparency and conductivity, was acquired from Ossila (UK) with a 1.1mm surface thickness. Solvents like analytical-grade chloroform and methanol were procured from Sigma-Aldrich and Laboratory Reagent India, respectively, ensuring high purity for device fabrication.

3. Experimental

3.1. Synthesis of Poly (3-hexylthiophene) (P3HT) and Polythiophene (PT)

The synthesis of the 3-hexylthiophene polymer involved several sequential steps. Initially, 0.84 gm of 3-hexylthiophene was mixed with 50 ml of chloroform ($CHCl_3$), and this mixture was degassed with nitrogen (N_2) for approximately 5 minutes. Subsequently, 1.62 gm of iron(III) chloride ($FeCl_3$) was dissolved in 50 ml of $CHCl_3$ then dropwise added to the degassed mixture.The reaction mixture was stirred continuously for 24 hours. After the stirring period, the mixture was washed in 100 ml of methanol, causing the 3-hexylthiophene polymer to precipitate. This process successfully yielded the desired poly (3-hexylthiophene). The same above procedure was used to prepare Polythiophene (PT) using thiophene monomer instead of 3- 3-hexyl thiophene monomer, as shown in Figure (1a, 1b, 1c, 1d) in detail.

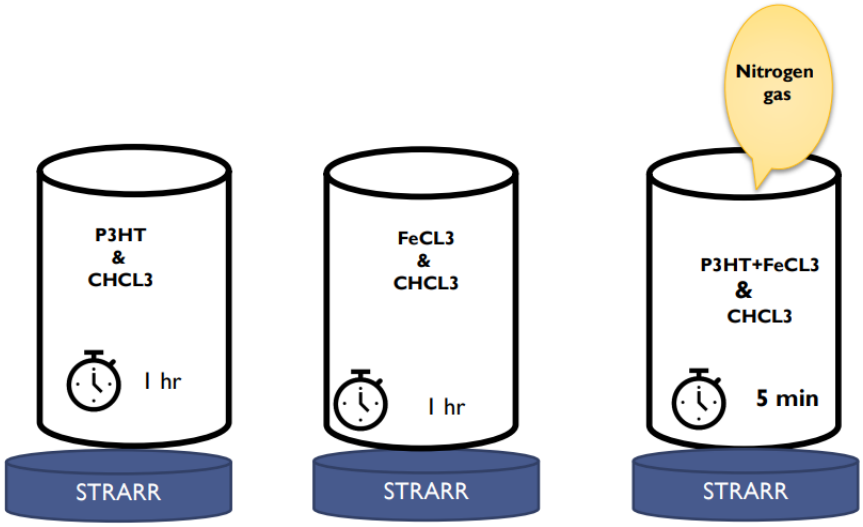

Fig. 1. (a): step (1)

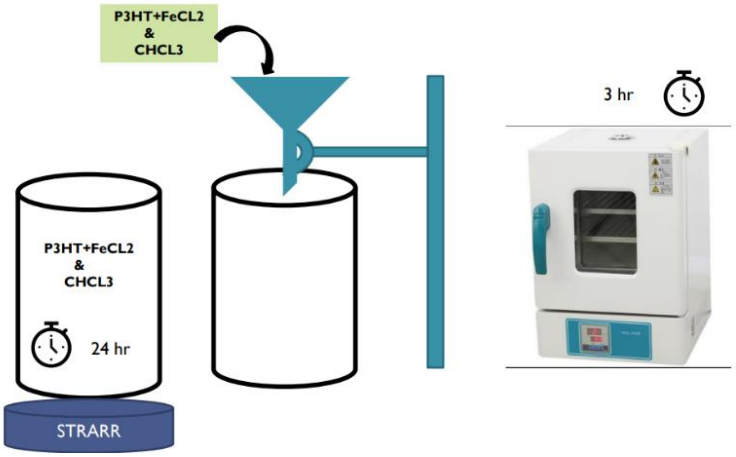

Fig. 1. (b): step (2)

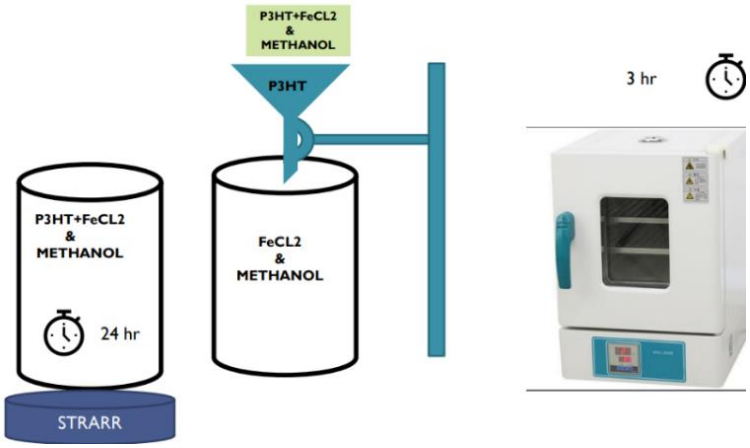

Fig. 1. (c): step (3)

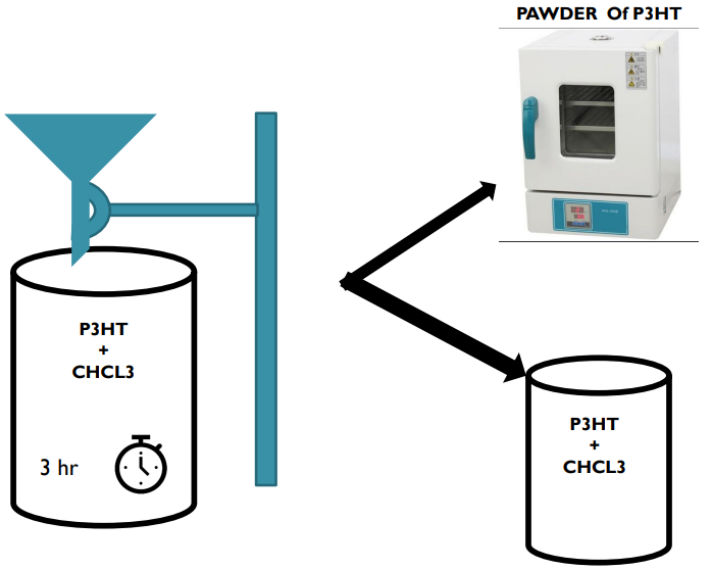

Fig. 1. (d): step (4)

3.2. Preparation of Poly(3-hexylthiophene - CO-Thiophene)

Poly (3-hexylthiophene-co-thiophene) were synthesized in the same above procedure using varying percentage ratios of 3-hexylthiophene and thiophene, Prepared by the addition polymerization method as outlined in Table 1.

Table 1. Show abbreviation symbols of prepared polymers and copolymers.

Polymers and copolymers	Abbreviation symbols
Poly3-hexyl thiophene (P3HT)	Polymer I
Poly thiophene (PT)	Polymer II
(50% P3HT-CO-50%PT)	Polymer III
(70% P3HT-CO-30%PT)	Polymer IV
(90% P3HT-CO-10%PT)	Polymer V

4. Preparing samples to study optical properties

A glass substrate was taken, and a layer of pre-prepared polymers was deposited on the glass substrate.

A thickness of polymer (10.04 x 10-5 m) was obtained, after which the optical properties were measured with an ultraviolet device, as shown in figure (2).

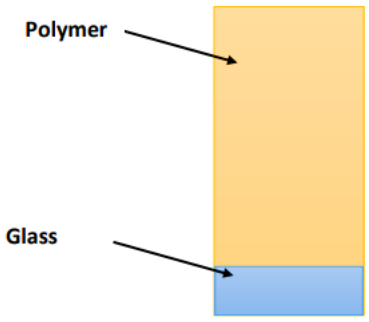

Fig. 2. Shows the glass and Polymer.

5. Results and discussion

5.1. Fourier Transform Infrared (FT-IR) spectrum of the P3HT

The infrared (IR) spectrum of poly 3-hexylthiophene (P3HT) fig (3) is depicted in the figure, revealing several functional groups and their corresponding vibrational frequencies as follows. A strong peak is observed at 3028 cm-1, which is attributed to the aromatic C-H stretching vibration of the thiophene ring, indicating the presence of aromatic carbon-hydrogen bonds. Additionally, two distinct peaks at 2885 cm-1 and 2773 cm-1 correspond to the stretching vibrations of aliphatic C-H bonds, signifying the presence of aliphatic hydrocarbon chains. The spectrum also displays a significant band at 1624 cm-1, corresponding to the stretching vibration of C=C double bonds, further confirming the existence of conjugated double bonds within the polymer structure. At 1176 cm-1, there is a distinct peak, indicating the presence of C-S stretching vibrations, characteristic of the thiophene ring. Lastly, a peak at 833 cm-1 corresponds to aromatic C-H out-of-plane vibrations, providing additional structural information about the P3HT molecule. The IR spectrum of P3HT offers valuable insights into its molecular composition and structure.

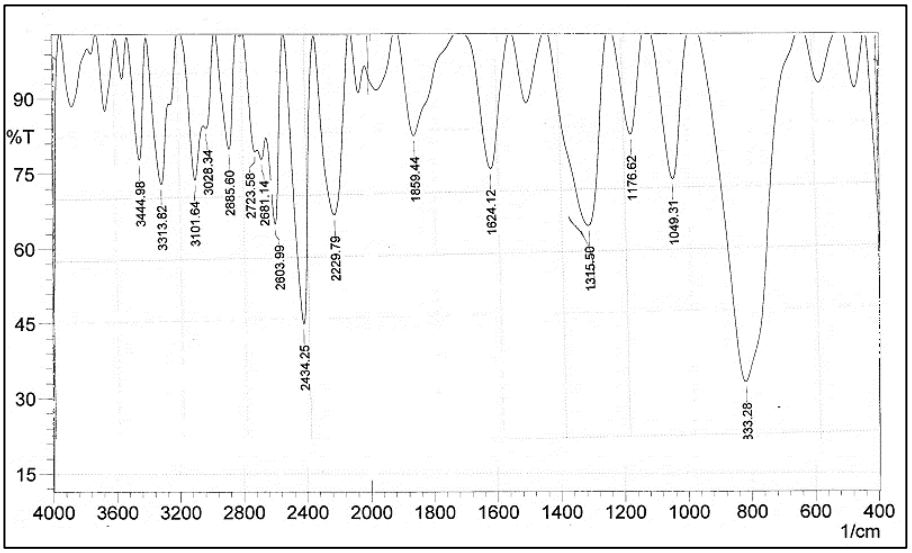

Fig. 3. Fourier Transform Infrared (FT-IR) Spectroscopy of (Polymer I)

5.1.1. Fourier Transform Infrared (FT-IR) spectrum of the Polythiophene

The infrared (IR) spectrum of polythiophene, as depicted in Figure (4), showed that the peak at 3028 cm-1 is attributed to the aromatic C-H stretching vibration of the thiophene ring, a key component of polythiophene's conjugated backbone. At 1646 cm-1, another prominent peak corresponds to the C=C stretching vibration, indicative of the conjugated double bonds within the polymer. The spectrum also features a distinctive peak at 783 cm-1, associated with the C-H bending mode, specifically the out-of-plane bending of carbon-hydrogen bonds. At 694 cm-1, a peak is observed, indicating C-S stretching vibrations in the presence of sulfur in the thiophene rings.

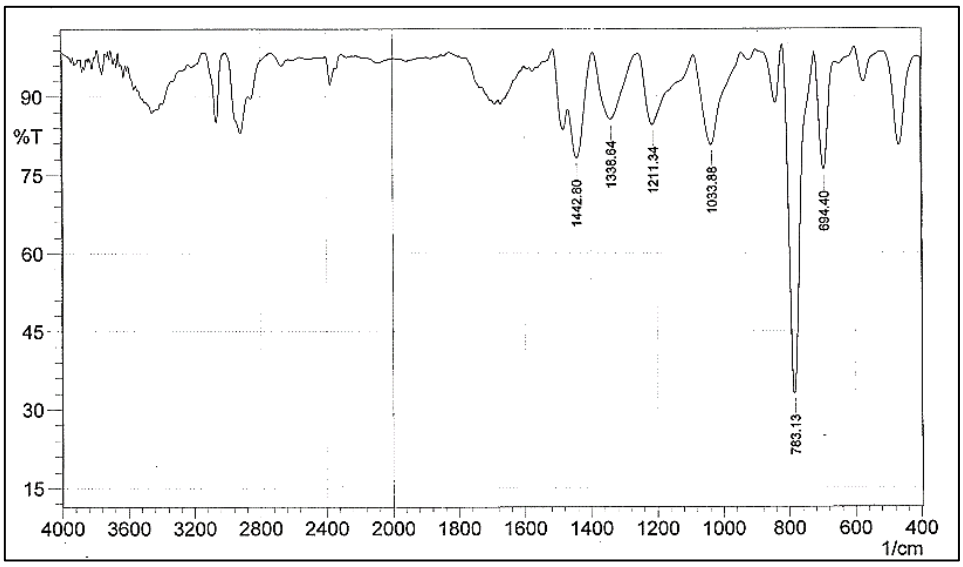

Fig. 4. Fourier Transform Infrared (FT-IR) Spectroscopy of (Polymer II)

5.1.2. Fourier Transform Infrared (FT-IR) spectrum of the copolymer

The FT-IR (Fourier Transform Infrared) spectrum of Poly (3HThiophene-CO-thiophene) in Figure (5) provides several peaks in the spectrum that are indicative of the various functional groups and chemical bonds present within the polymer chain. At 3054 cm-1, we observe a strong absorption peak corresponding to the aromatic C-H stretching vibrations of the thiophene ring, confirming the presence of this aromatic moiety in the polymer. The 2916 cm-1 and 2850 cm-1 peaks are associated with stretching vibrations of aliphatic C-H bonds, likely originating from the methylene groups within the polymer. The appearance of a peak at 1311 cm-1 indicates methylene bending vibrations, suggesting a degree of conformational flexibility within the polymer chain. The absorption band at 1138 cm-1 is attributed to C-S stretching vibrations, confirming the presence of sulfur atoms in the polymer structure. Additionally, peaks at 783 cm-1 and 656 cm-1 are observed, with the former corresponding to vibrations related to hexyl substitution of the methylene group and the latter associated with C-S stretching vibrations of the thiophene ring. Together, this FT-IR spectrum provides a comprehensive fingerprint of the Poly (3HT-CO-thiophene) and aids in its structural characterization.

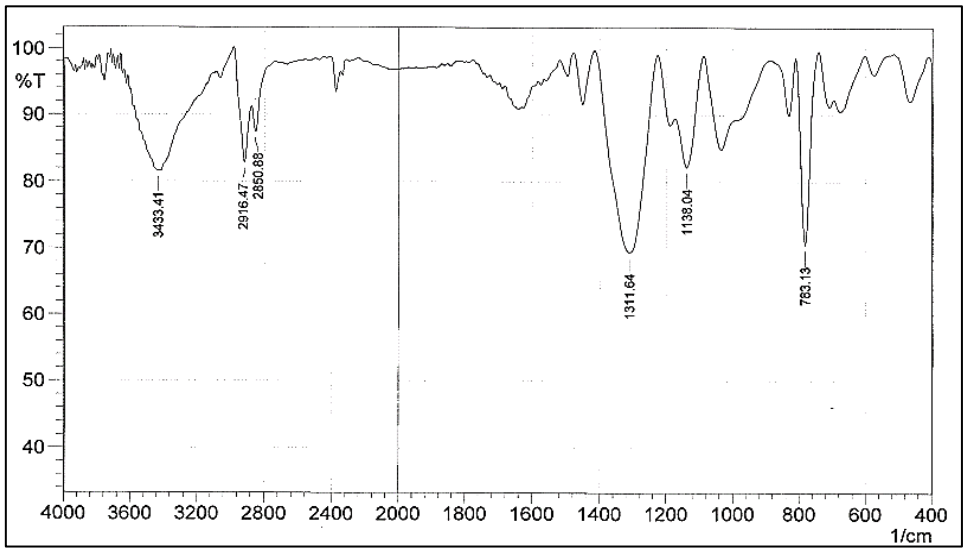

Fig. 5. FT-IR Spectroscopy of copolymer

5.2. Scanning Electron Microscopy Analysis of P3HT Films

Fig. (6) provides scanning electron microscope (SEM) images of the copolymers. These images visually represent the SEM measurements performed on the sample. It reveals the presence of an intermediate layer within the heterogeneous junction. This intermediate layer displays a cross-linked network formation throughout the active layer, resulting in a textured surface with uniformly distributed scale-like granules. After a careful and detailed examination of the samples, the results yielded interesting insights. The results showed that the dimensional range of the prepared samples was within the nanoscale range of less than 100 nm, with the minimum value reaching 45.556 nm for the sample (Polymer V). The upper limit value is 79.479 nm for the sample (Polymer II). This nanoscale size range is crucial because it classifies the layer as having the ability to absorb a large amount of light [24].

SEM analysis provides a visual glimpse into the structure of copolymers and valuable data on the thickness and properties of the polymer layer, which plays an essential role in the light transmission properties.

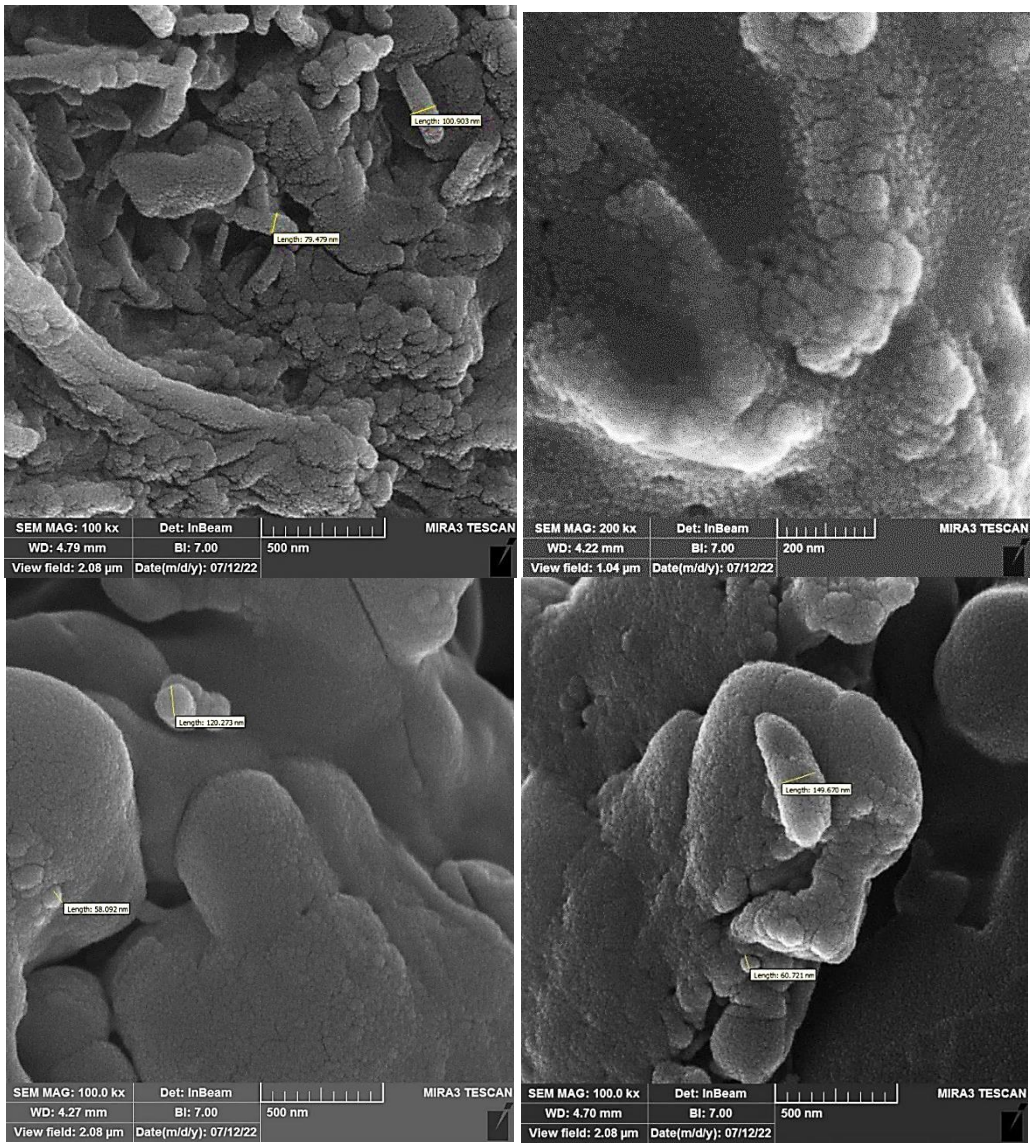

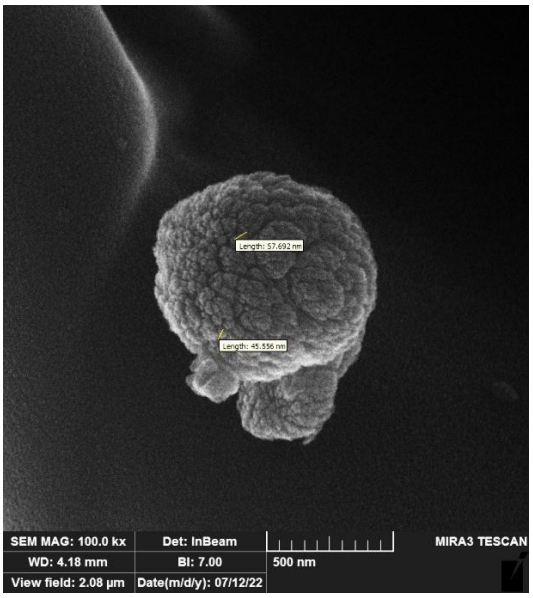

Fig. 6. Scanning Electron Microscopy of a) Polymer I; b) Polymer II; c) Polymer III; d) Polymer IV; e) Polymer V

5.3. Atomic Force Microscopy (AFM) Analysis

We used an atomic force microscope from the University Of Tehran, Iran (Newport Multimode™ Model 401). The surface properties of pure and copolymer polymers were studied, and these samples were prepared and deposited precisely on silicon substrates. During the measurement process, an atomic force microscope (AFM) tip mode was used. Fig. (7- 11) showed samples taken using AFM. Each image takes a different dimension of the polymeric surfaces within (10 nm). These measurements were conducted under standard environmental conditions.

The pictures provide interesting details. It is worth noting that the images show different aggregates of atoms and molecules, and these differences are due to the binding energy of the chemical bonds within the polymer's structure.

In addition, AFM imaging gives us a deep insight into the three-dimensional structure of the polymeric membrane, providing a comprehensive examination of the thickness and roughness of the samples as well as giving valuable information about the surface properties of the films including the distribution of grain sizes and the presence of atomic clusters, all of which contribute to a comprehensive understanding of the properties of the material. And potential applications.

The results recorded a thickness ranging from approximately 49.1 to 10.2 nanometres [25]. The recorded roughness of the polymer surfaces ranged from 20.7 nanometres to 5.19 nanometres, as shown in the table (2). It was compared with some published research [25], [26]

Table 2. Table showing roughness and thickness values of Sample

Roughness nm	Thickness nm	Sample
11.7	25.8	Polymer I
10.4	20.6	Polymer II
5.19	10.2	Polymer III
20.7	49.1	Polymer IV
14.3	36.1	Polymer V

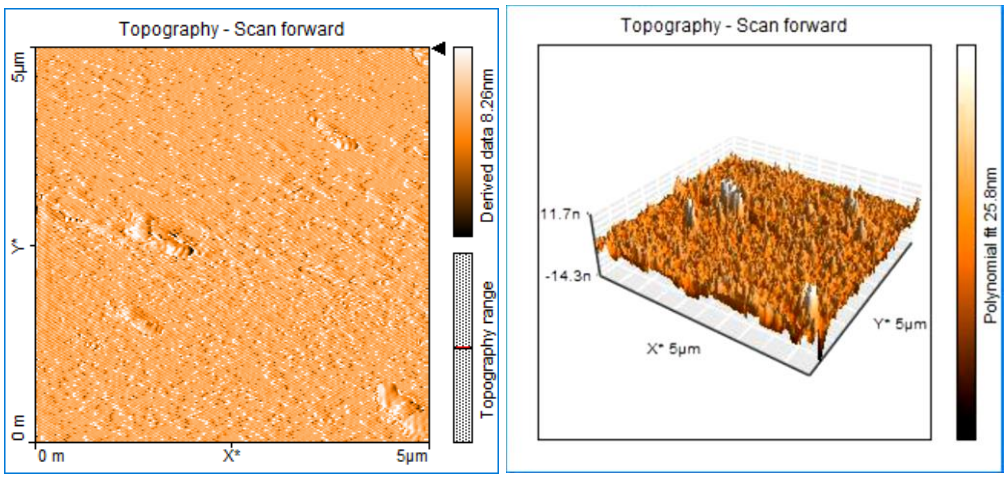

Fig.7. Atomic force microscope (AFM) of Polymer I

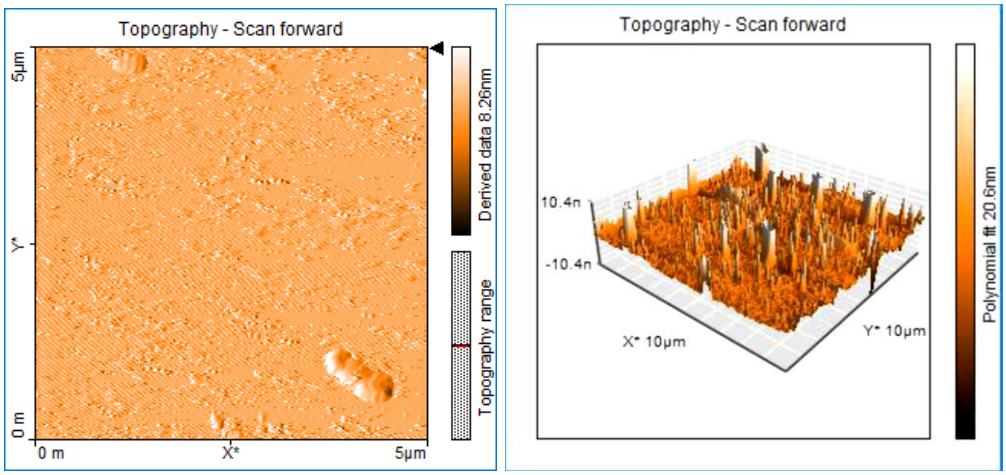

Fig.8. Atomic force microscope (AFM) of Polymer II

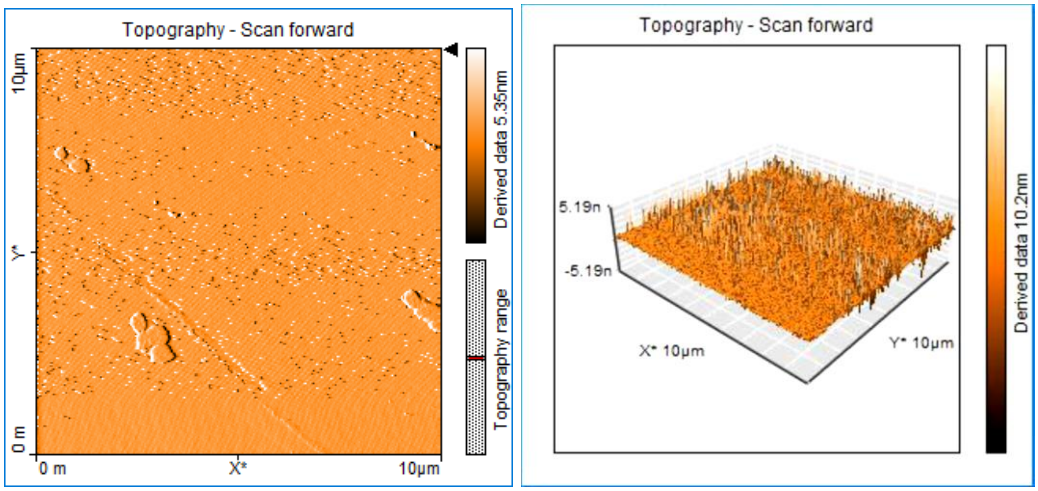

Fig.9. Atomic force microscope (AFM) of Polymer III

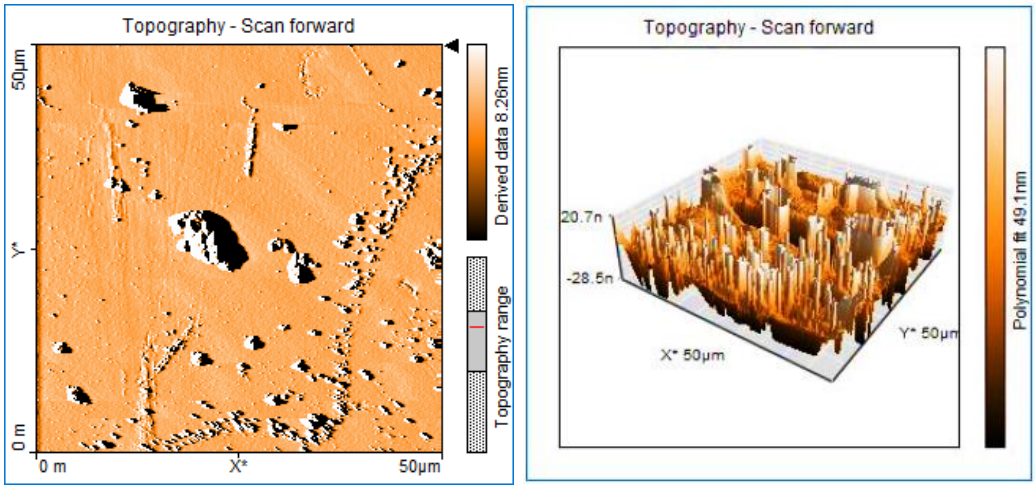

Fig. 10. Atomic force microscope (AFM) of Polymer IV

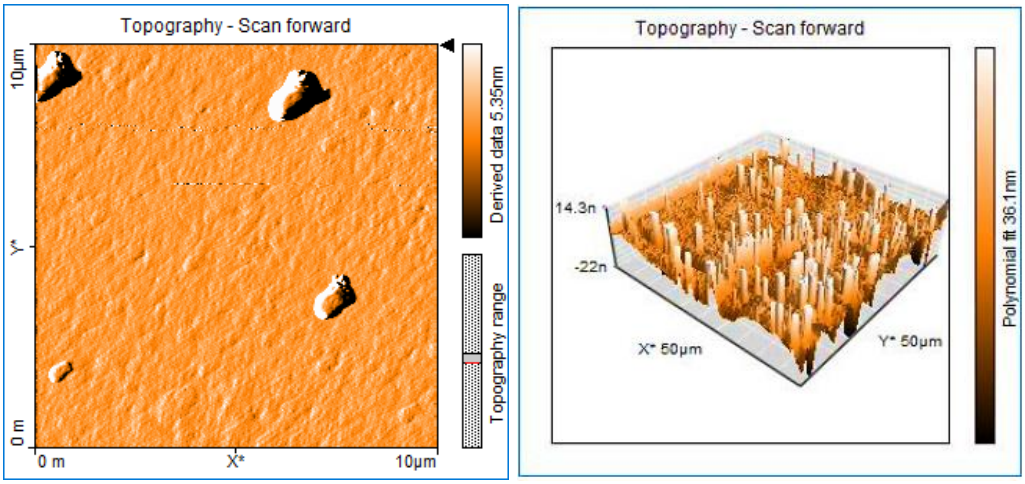

Fig. 11. Atomic force microscope (AFM) of Polymer V

5.4. X-Ray Diffraction (XRD) Analysis

We used an X-ray diffraction device from the University of Tehran, Iran. The study used X-ray diffraction (XRD) to examine material structures fig (12-16) to reveal several key insights. Due to their low X-ray absorption, polymers allow minimal interference, yet even highly crystalline ones contain amorphous regions owing to inherent structural irregularities.

Due to these complexities, achieving a completely monocrystalline polymer structure is challenging. Broad XRD peaks indicate structural defects within polymers, while higher polymer crystallinity necessitates high viscosity and low permeability for a more ordered molecular arrangement. Specific XRD patterns of P3HT and Thiophene indicated crystallinity in P3HT and an amorphous structure in Thiophene. Quantitative peak data provided crucial insights into material, crystalline properties, enabling the distinction between crystalline and amorphous phases and offering valuable information on material structural behaviors.

The X-ray analysis results shown in tables (3 to 6) obtained the crystal lattice parameter, which is identical to the sources [27], [28], [29], [30], [31]. The X-ray diffraction pattern of the formed copolymers is shown in Figures (12 to 16). Several Bragg reflection peaks were observed at values of 2θ shown in Table (3 -7); the crystal lattice parameter was obtained, and these results are identical to the sources [27], [28], [29], [30], [31], [32], [33], [34], [35].

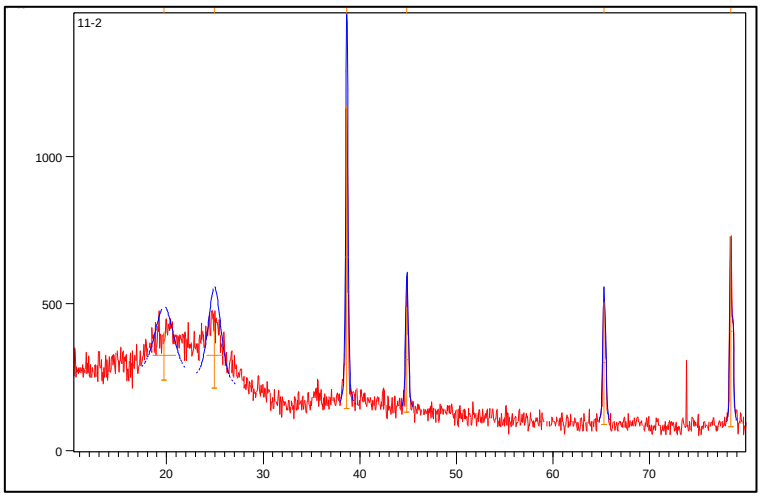

Fig. 12 X-Ray Diffraction of Polymer I

Table 3. X-ray diffraction data for Polymer I

Pos. [°2Th.]	Height [cts]	FWHM [°2Th.]	d-spacing [Å]	number of Bragg reflection	Tip Width
19.73422	165.3736	2.3616	4.49884	211	2.8339
24.93554	225.3268	1.5744	3.57096	100	1.8893
38.62958	1026.05	0.246	2.33082	200	0.2952
44.84426	359.1008	0.2952	2.02119	142	0.3542
65.2434	419.373	0.246	1.43007	200	0.2952
78.39391	647.5464	0.1968	1.21986	311	0.2362

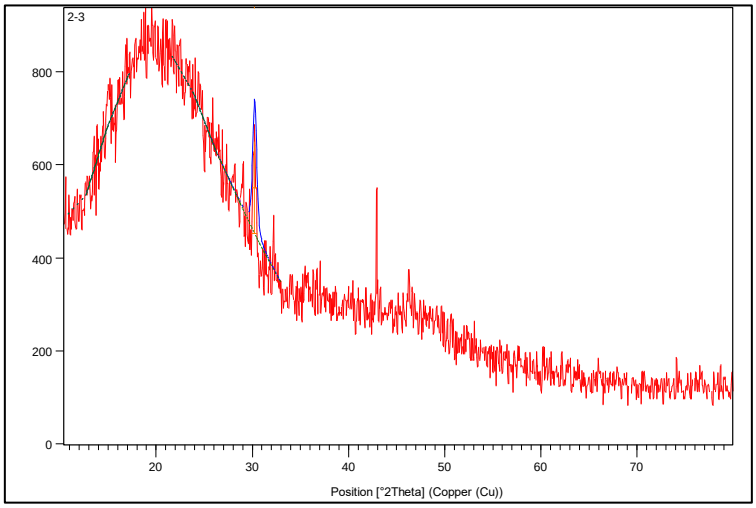

Fig. 13. X-Ray Diffraction of Polymer II

Table 4. X-ray diffraction data for Polymer II

Pos. [°2Th.]	Height [cts]	FWHM °2Th.]	d-spacing [Å]	number of Bragg reflection	Tip Width
30.22519	198.7349	0.48	2.95454	111	0.576

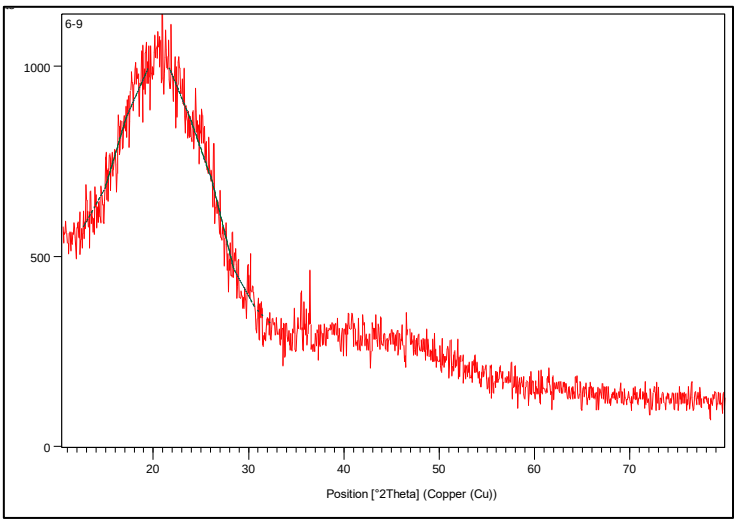

Fig. 14. X-Ray Diffraction of Polymer III

Table 5. X-ray diffraction data for Polymer II

Pos. [°2Th.]	Height [cts]	FWHM [°2Th.]	d-spacing [Å]	number of Bragg reflection	Tip Width
22.02519	193.2349	0.36	2.15454	110	0.476

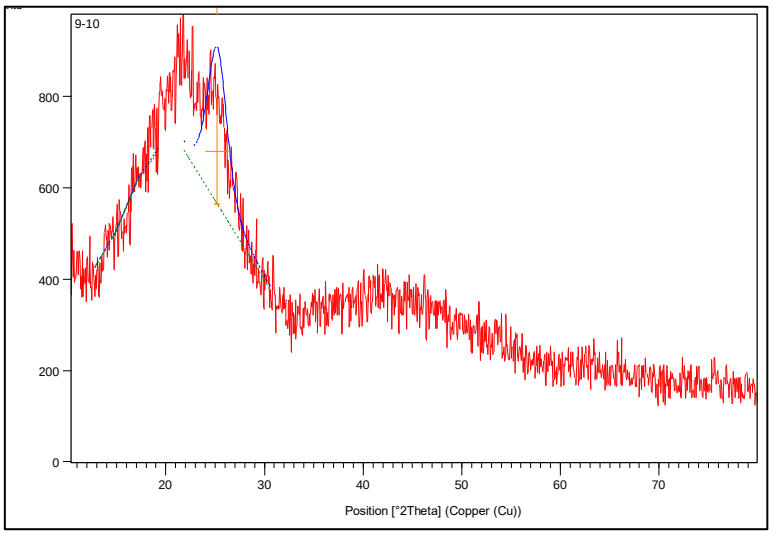

Fig. 15 X-Ray Diffraction of Polymer IV

Table 6. X-ray diffraction data for Polymer IV

Pos. [°2Th.]	Height [cts]	FWHM [°2Th.]	d-spacing [Å]	Number of Bragg reflection	Tip Width
25.19181	230.0692	2.4	3.53229	110	2.88

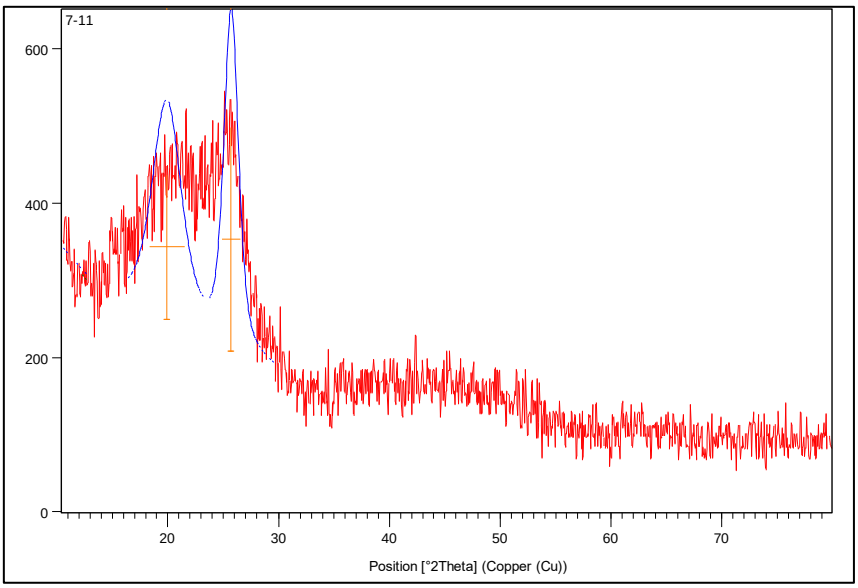

Fig. 16 X-Ray Diffraction of Polymer V

Table 7. X-ray diffraction data for Polymer V

Pos. [°2Th.]	Height [cts]	FWHM [°2Th.]	d-spacing [Å]	number of Bragg reflection	Tip Width
19.89935	187.6678	3.1488	4.46188	211	3.7786
25.70795	290.4137	1.5744	3.4654	111	1.8893

5.5. Optical Properties

Our research, conducted with the utmost precision, utilized a UV device from the University of Basra, College of Education for Pure Sciences, Department of Physics (Shimadzu corporation Japan, UV-1800 240V).

Copolymer films were deposited onto a glass substrate after annealing at 50 0C for 60 min in the wavelength between 250 - 750 nm. The central absorption wavelength region of samples Polymer I, Polymer IV, and Polymer V is around λ~ 490 nm. All films' UV- UV-absorption spectra were plotted in Figure (17) and featured absorption bands around λ~470 nm, 510 nm, and 490 nm, respectively. While the central absorption wavelength region for samples Polymer II and Polymer III is about 390 nm~, the ultraviolet absorption spectra of the two samples were plotted in Figure (17), and there was a remarkable similarity in the peaks due to the high overlap ratio of Polymer II. The central peak at ~490 nm is attributed to the π–π* transition in the π–π crystal stacking structure of the Polymer I (conjugated polymer) polymer chains [36].

Our thorough data analysis included drawing the relationship between the samples' absorption coefficient and photon energy. The absorption coefficient value was more significant than (10 4 cm-1), indicating that the transition was a direct electron transfer.

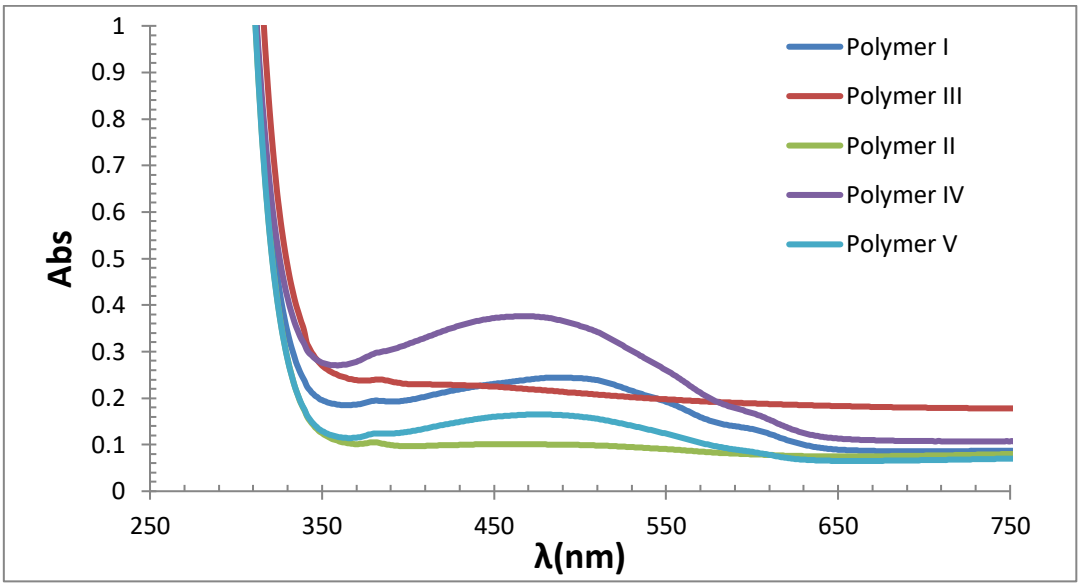

Fig. 17. Absorption of Polymer (I - V) with the wavelength

Figures 18 presented illustrate the relationship between (hν) vs. (hνα) 2 and the photon energy of the samples. The energy gap was determined by identifying the intersection point of the linear relationship with hν yielding values of approximately)2.78 eV for Polymer I, 2.3 eV for Polymer II and 1.88eV for Polymer III , and 1.9 eV for Polymer IV and 2.05 eV for Polymer V.

Table 8: Shows the energy gap values for different samples. It is worth noting that there is a clear trend from the numbers, as the energy gap decreases when preparing the composite polymers, as it decreases from (2.78eV) (2.3 eV) to (1.88 eV). This indicates a lower energy gap of 1.88 eV after doping.

The decrease in the energy gap is due to the increase in the percentage of polymeric overlay. As doping levels increase, polar states enter the energy gap, eventually leading to its contraction [37].

Moreover, the increased absorption coefficient observed with increasing polymer overlay ratio can be attributed to the absorption of additional photons by the newly generated energy levels within the gap. These levels multiply in number as doping levels rise, contributing to increased absorption coefficients [38]. Analysis of optical properties, precisely the energy gap and absorption coefficients, provides valuable insights into the effect of increasing the proportion of polymeric overlay on the material's electronic structure, highlighting its potential applications in solar cells [39].

Table 8. The energy gap of the samples

samples	symbol	E.g. (eV)
Poly3-hexyl thiophene (P3HT)	Polymer I	2.78
Poly thiophene (PT)	Polymer II	2.3
(50% P3HT-CO-50%PTH)	Polymer III	1.9
(70% P3HT-CO-30%PTH)	Polymer IV	1.88
(90% P3HT-CO-10%PTH)	Polymer V	2.05

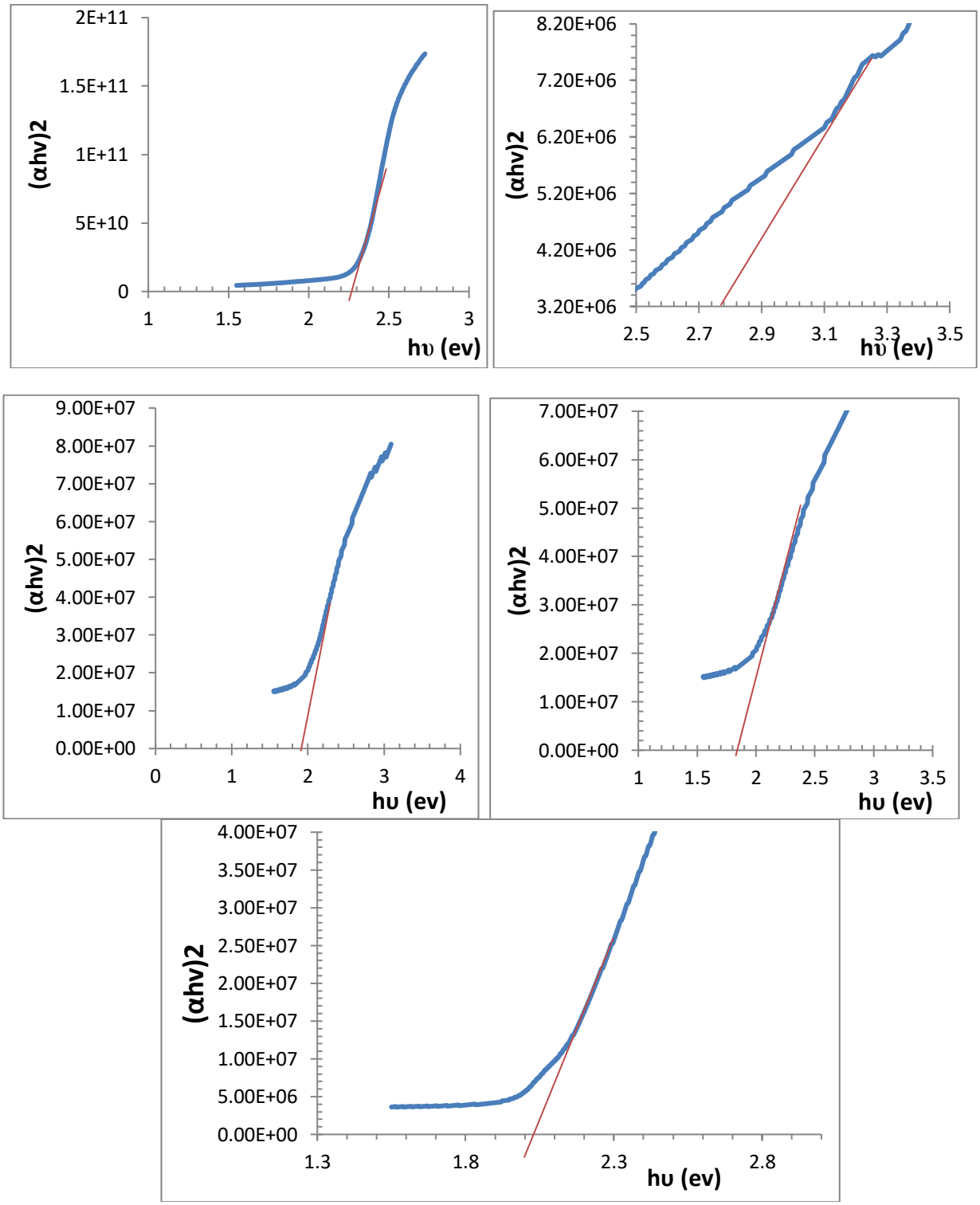

Fig. 18. Band gab Energy Of: a) Polymer I; b) Polymer II; c) Polymer III; d) Polymer IV; e) Polymer V A single oscillator Model can analyze The refractive index dispersion [40].

$$n^2 + 1 = \frac{E_d + E_o}{{E_o}^2 - (h\nu)^2} \tag{5}$$

Where n is the refractive index, h is Planck's constant, ν is the frequency, (hν) is the photon energy, Eo is the average excitation energy for electronic transitions, and Ed is the dispersion energy, which is a measure of the strength of interbond optical transitions. From the drawing between ($\frac{1}{n^2-1}$) versus (hν) 2 Fig (from 19). The oscillator parameters E o and E d values were determined from the

slope (Eo Ed)-1 and the intercept (E0/Ed) on the vertical axis, respectively. From there, it was determined the values of the oscillator parameters (Eo and Ed) were; a noticeable increase in the values of (Eo) and a decrease in the values of (Ed) were observed. The oscillator energy, Eo, is related to the optical band gap.

Tabulated in table (9). It is known that inter-material boundaries contain structural defects and impurities. These factors have a strong influence on the absorption processes [41].

Table 9. The values of the oscillator parameters (Eo and Ed)

symbol	E_o (eV)	E_d (eV)
Polymer I	0.925	1.098
Polymer II	0.944	1.049
Polymer III	1.34	0.302
Polymer IV	1.428	0.297
Polymer V	1.471	0.199

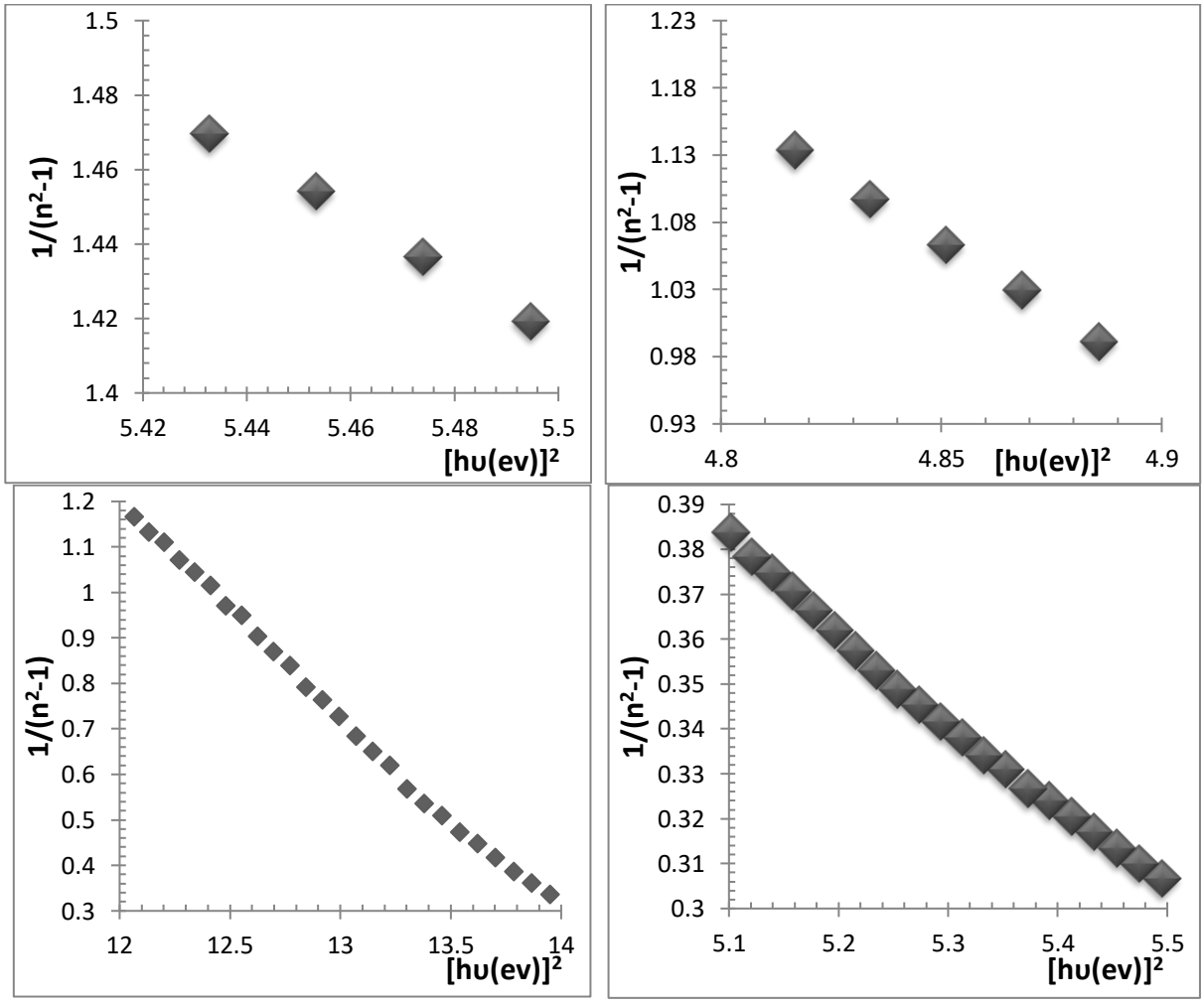

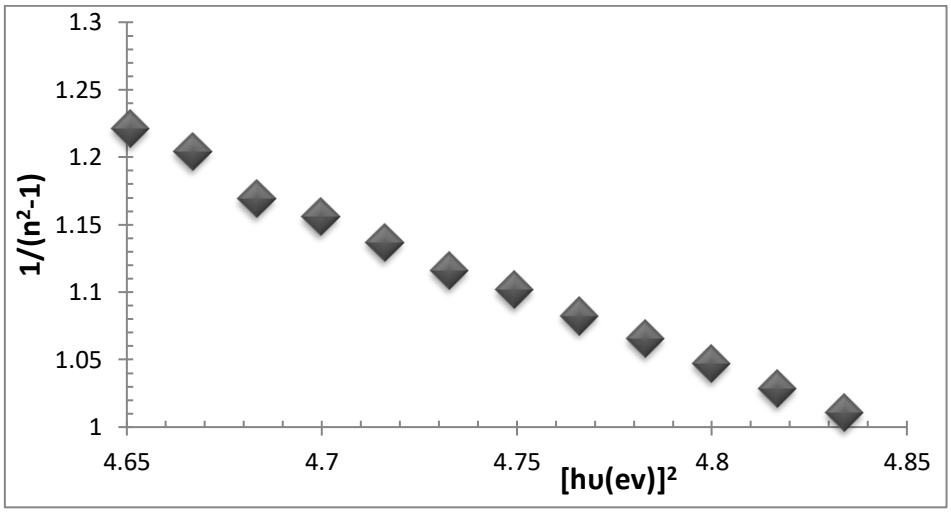

Fig. 19. Relationship between ($\frac{1}{n^2-1}$) versus (hν) ^{2} of: a) Polymer I; b) Polymer II; c) Polymer III; d) Polymer IV; e) Polymer V

The long wavelength refractive index (n∞), average oscillator wavelength (λo), and oscillator length strength So can be estimated by the single oscillator model given by [42].

$$\frac{n_\infty^2-1}{n^2-1} = 1 - \frac{\lambda_o^2}{\lambda^2} \quad (6)$$

n∞ Value was obtained from the linear parts of ($\frac{1}{n^2-1}$) and. ($\frac{1}{\lambda^2}$). Figure (20) from the curve plotted are given in Table (10). Eq. (6) becomes:-

$$n^2 - 1 = \frac{s_o\lambda^2}{1-\frac{\lambda_o^2}{\lambda^2}} \quad (7)$$

S0 = (n ∞ -1)/λ2 is the average oscillator parameter, which is the strength of the individual dipole oscillator. The So value was estimated using Eq. above and is given in table (10).

The M-1 and M-2 moments of the optical spectra are expressed as [43].

$$E_o^2 =, E_d^2 = \frac{M_{-1}^3}{M_{-1}} \quad (8)$$

The M-1 and M-3 moments were estimated using the above equation and are in Table (10). The M-1 and M-2 moments changed due to the formation coordination of the complex. The third-order nonlinear susceptibility (χ 3) has been calculated from the following equation (8) and tabulated in Table (10).

$$X^3 = A\left[\left(\frac{E_o E_d}{4\pi(E_o^2-(h\nu)^2}\right)^4\right] = \frac{\mathbf{A}}{(\mathbf{4\pi})^4\,(\mathbf{n^2-1})^4} \quad (9)$$

It is noted from Table (10) that the values of the refractive index no2 decrease with the decrease in Ed and the increase in EO, and the increase in the dielectric constant ε∞ when the wavelength decreases.

Likewise, a decrease in the values of the average strength of the position of the oscillation SO was observed. In contrast, the values of the average position of the oscillation λo increased with the decrease of Ed and the increase of EO.

The provided table encapsulates essential optical properties of diverse materials and compositions at distinct wavelengths and energy levels. Each entry delineates parameters crucial in understanding the materials' response to light, encompassing nonlinear optical behavior (Third-order visual effect X3, The Average Oscillator So), energy-related characteristics (Moments Of The Optical Spectra For Liquid Crystal M-3, Moments Of The Optical Spectra For Liquid Crystal M-1, and key optical traits (refractive index, energy dissipation, band gap energy). For instance, P3HT showcases moderate values across parameters, indicating its potential in specific electronic applications with a

band gap energy (Eg) of 2.78 eV for Polymer I. Conversely, Polythiophene demonstrates differing optical traits, notably with an Eg of 2.3 eV for Polymer II. Furthermore, it showcases sensitivity to compositional changes. These findings suggest potential applications in optoelectronics and photonics, implying materials with specific band gap energies may suit distinct uses like solar cells or light-emitting devices. However, further analysis and experimentation are warranted to unravel these materials' full implications and applications based on their intricate optical properties [44].

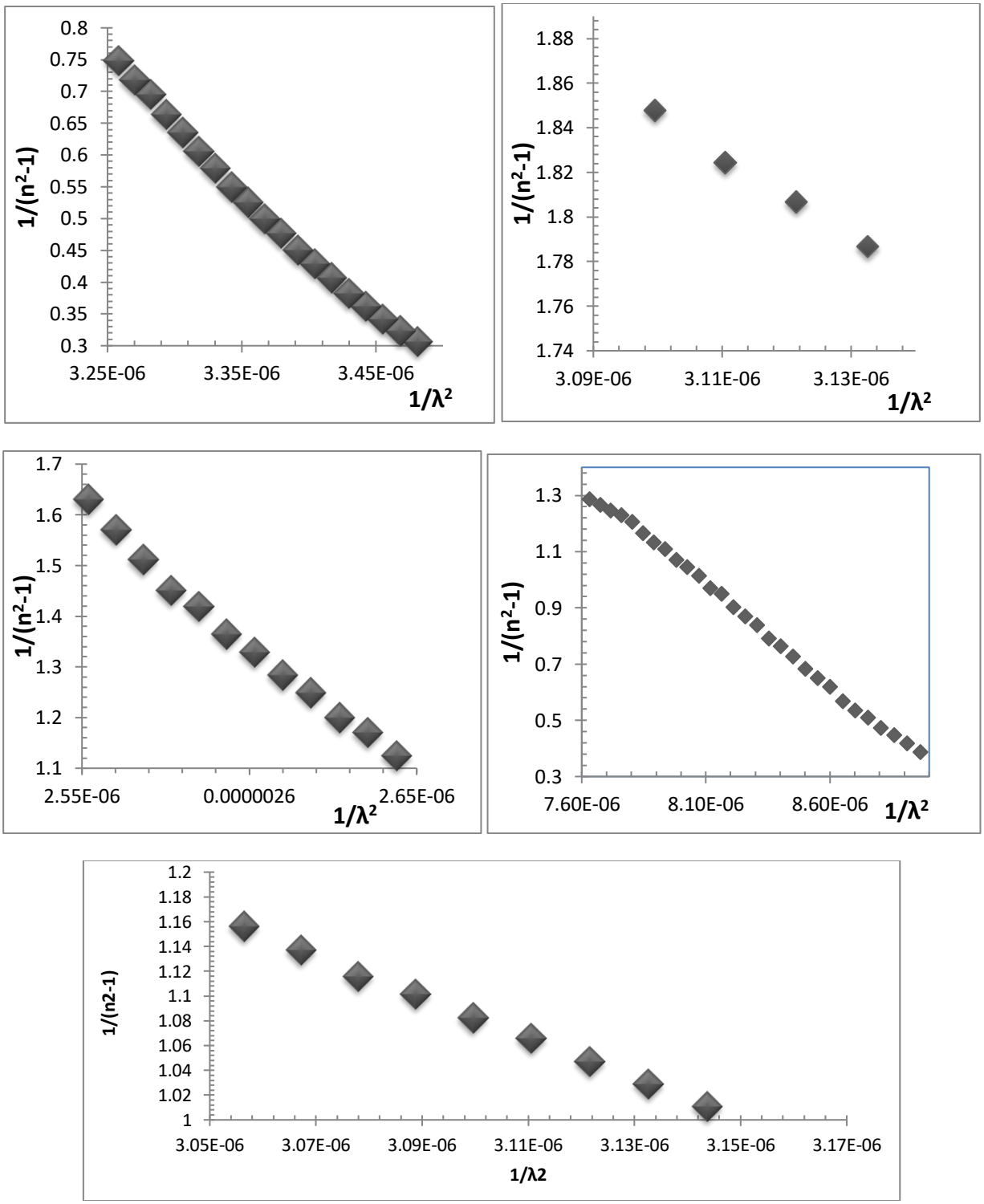

Fig. 20. Relationship between ($\frac{1}{n^2-1}$) versus ($\frac{1}{\lambda^2}$) of: a) Polymer I; b) Polymer II; c) Polymer III; d) Polymer IV; e) Polymer V

Table 10. Parameters some optical properties.

Symbol	no2	ε∞	M-1	M-3	So 10^{-7}	X3 10^{-24}	λo (nm)
Polymer I	1.4	1.0728	0.923	0.769	47.9	9.6	442.93
Polymer II	1.382	1.0954	0.56	0.714	13.25	7.52	603.23
Polymer III	1.21	1.26	0.211	0.165	4.2	2.819	952.698
Polymer IV	1.153	1.271	0.2	0.1443	3.84	2.08	1095.94
Polymer V	1.132	1.297	0.151	0.0887	1.9	2.04	1099

6. Conclusion

This study aims to investigate tthe effect of the copolymer ratio on the optical properties that can be used in solar cell applications. The copolymers were prepared by additive polymerization. The samples were diagnosed, and the X-ray examination showed that the samples prepared from pure and composite polymers possess a high degree of crystallinity. The above models were also characterized by FT-IR spectroscopy, which showed that these films have clear active groups. The optical properties of all prepared films were also studied, such as absorbance within the spectral range (200 - 800 nm) as a function of wavelength, energy gap, dispersion energy, single oscillation energy, refractive index, dielectric constant at high frequencies E∞, and momentum coefficients M-1 M-3. , the visual impact of the third degree x3. The study showed that the absorption spectrum of the films of the materials under study falls within the visible spectrum region, where the highest peak was recorded for pure and copolymers at the wavelength of 485 – 495 nm. The study showed that the optical energy gap for the P3HT polymer is (2.78 eV) and for thiophene (2.3 eV), and the value of the gap decreases with increasing doping rate until it reaches (1.88 eV) at the copolymer rate of 70% P3HT and 30%. The thickness of the film varied from 49.1 to 10.2 nm, and the recorded roughness of the polymer surfaces ranged from 20.7 nm to 5.19 nm.

References

[1] N. Tessler, V. Medvedev, M. Kazes, S. Kan, and U. Banin, “Efficient near-infrared polymer nanocrystal light-emitting diodes,” Science (80-.)., vol. 295, no. 5559, pp. 1506–1508, 2002.

[2] C. Yoon, K. P. Yang, J. Kim, K. Shin, and K. Lee, “Fabrication of highly transparent and luminescent quantum dot/polymer nanocomposite for light emitting diode using amphiphilic polymer-modified quantum dots,” Chem. Eng. J., vol. 382, p. 122792, 2020.

[3] A. V. Kesavan, M. P. Kumar, A. D. Rao, and P. C. Ramamurthy, “Light management through up-conversion and scattering mechanism of rare earth nanoparticle in polymer photovoltaics,” Opt. Mater. (Amst)., vol. 94, pp. 286–293, 2019.

[4] A. Benchaabane et al., “Effect of OA-ZnSe nanoparticles incorporation on the performance of PVK organic photovoltaic cells,” Mater. Sci. Semicond. Process., vol. 64, pp. 115–123, 2017.

[5] G. Jiang, A. S. Susha, A. A. Lutich, F. D. Stefani, J. Feldmann, and A. L. Rogach, “Cascaded FRET in Conjugated Polymer/Quantum Dot/Dye-Labeled DNA Complexes for DNA Hybridization Detection,” ACS Nano, vol. 3, no. 12, pp. 4127–4131, 2009, Doi: 10.1021/nn901324y.

[6] P. Reiss, E. Couderc, J. De Girolamo, and A. Pron, “Conjugated polymers/semiconductor nanocrystals hybrid materials—preparation, electrical transport properties and applications,” Nanoscale, vol. 3, no. 2, pp. 446–489, 2011.

[7] S. A. McDonald et al., “Solution-processed PbS quantum dot infrared photodetectors and photovoltaics,” Nat. Mater., vol. 4, no. 2, pp. 138–142, 2005, Doi: 10.1038/nmat1299.

[8] Y. Wu, X. Wu, F. Yang, and J. Ye, “Preparation and characterization of waterborne UV lacquer product modified by zinc oxide with flower shape,” Polymers (Basel)., vol. 12, no. 3, p. 668, 2020.

[9] D. S. Koktysh et al., “Near-Infrared Electroluminescence from HgTe Nanocrystals,” ChemPhysChem, vol. 5, no. 9, pp. 1435–1438, 2004, Doi: 10.1002/cphc.200400178.

[10] S. Ananthakumar, J. Ramkumar, and S. Moorthy Babu, “Synthesis of thiol modified CdSe nanoparticles/P3HT blends for hybrid solar cell structures,” Mater. Sci. Semicond. Process., vol.

22, pp. 44–49, 2014, Doi: 10.1016/j.mssp.2014.02.008.
[11] A. K. Diallo, M. Gaceur, N. Berton, O. Margeat, J. Ackermann, and C. Videlot-Ackermann, "Towards solution-processed ambipolar hybrid thin-film transistors based on ZnO nanoparticles and P3HT polymer," Superlattices Microstruct., vol. 58, pp. 144–153, 2013, Doi: 10.1016/j.spmi.2013.03.012.
[12] W. L. Leong, P. S. Lee, S. G. Mhaisalkar, T. P. Chen, and A. Dodabalapur, "Charging phenomena in pentacene-gold nanoparticle memory device," Appl. Phys. Lett., vol. 90, no. 4, 2007, Doi: 10.1063/1.2435598.
[13] D.-I. Son et al., "Nonvolatile flexible organic bistable devices fabricated utilizing CdSe/ZnS nanoparticles embedded in a conducting polyN-vinylcarbazole polymer layer," Nanotechnology, vol. 19, no. 5, p. 55204, 2008, Doi: 10.1088/0957-4484/19/05/055204.
[14] M. Vilkman, K. Solehmainen, A. Laiho, H. G. O. Sandberg, and O. Ikkala, "Negative differential resistance in polymeric memory devices containing disordered block copolymers with semiconducting block," Org. Electron., vol. 10, no. 8, pp. 1478–1482, 2009, Doi: 10.1016/j.orgel.2009.08.012.
[15] B. Cho, T.-W. Kim, M. Choe, G. Wang, S. Song, and T. Lee, "Unipolar nonvolatile memory devices with composites of poly(9-vinylcarbazole) and titanium dioxide nanoparticles," Org. Electron., vol. 10, no. 3, pp. 473–477, 2009, Doi: 10.1016/j.orgel.2009.02.001.
[16] W. Tao and Y. Du, "The optical properties of solar cells before and after encapsulation," Sol. Energy, vol. 122, pp. 718–726, 2015.
[17] A. M. G. da Silva, K. de A. Barcelos, M. C. da Silva, and C. L. Morelli, "Blend of recycled poly (ethylene terephthalate) and polycarbonate with polyaniline for antistatic packaging," Polym. Polym. Compos., vol. 28, no. 5, pp. 331–337, 2020.
[18] A. A. Hussein, A. A. Sultan, M. T. Obeid, A. T. Abdulnabi, and M. T. Ali, "Synthesis and Characterization of poly (3-hexylthiophene)," Int. J. Sci. Eng. Appl. Sci. (IJSEAS)-Volume-1, Issue-7, 2015.
[19]N. Shrivastav, J. Madan, and R. Pandey, "A short study on recently developed tandem solar cells," Mater. Today Proc., 2023.
[20] T. Torimoto, T. Kameyama, T. Uematsu, and S. Kuwabata, "Controlling optical properties and electronic energy structure of I–III–VI semiconductor quantum dots for improving their photofunctions," J. Photochem. Photobiol. C Photochem. Rev., vol. 54, p. 100569, 2023.
[21] N. Baig, I. Kammakakam, and W. Falath, "Nanomaterials: A review of synthesis methods, properties, recent progress, and challenges," Mater. Adv., vol. 2, no. 6, pp. 1821–1871, 2021.
[22] I. Naji And A. Muslim, "The Influence Of Heat Treatment On The Characteristic Of Poly (3-Hexylthiophene-2, 5-Diyl) P3ht And):[6, 6] Phenyl-C71-Butyric Acid Methyl Ester (Pcbm) Blend," Dig. J. Nanomater. Biostructures, vol. 14, pp. 775–787, 2019.
[23] R. Cheng and Y. Guo, "Study on the effect of heat treatment on amethyst color and the cause of coloration," Sci. Rep., vol. 10, no. 1, p. 14927, 2020.
[24] I. Khan, K. Saeed, and I. Khan, "Nanoparticles: Properties, applications and toxicities," Arab. J. Chem., vol. 12, no. 7, pp. 908–931, 2019.
[25] L. Liirò-Peluso, J. Wrigley, D. B. Amabilino, and P. H. Beton, "Submolecular resolution imaging of P3HT: PCBM nanostructured films by atomic force microscopy: implications for organic solar cells," ACS Appl. nano Mater., vol. 5, no. 10, pp. 13794–13804, 2022.
[26] B. K. Kuila, A. Garai, and A. K. Nandi, "Synthesis, optical, and electrical characterization of organically soluble silver nanoparticles and their poly (3-hexylthiophene) nanocomposites: Enhanced luminescence property in the nanocomposite thin films," Chem. Mater., vol. 19, no. 22, pp. 5443–5452, 2007.
[27] E. Ercan, Y. Lin, L. Hsu, C. Chen, and W. Chen, "Multilevel photonic transistor memory devices based on 1D electrospun semiconducting polymer/perovskite composite nanofibers," Adv. Mater. Technol., vol. 6, no. 8, p. 2100080, 2021.
[28] R. Nandanwar, P. Singh, and F. Z. Haque, "Synthesis and characterization of SiO2 nanoparticles by sol-gel process and its degradation of methylene blue," Am. Chem. Sci. J, vol. 5, no. 1, pp. 1–10, 2015.
[29] A. Khorsand Zak, W. H. Abd. Majid, M. E. Abrishami, and R. Yousefi, "X-ray analysis of ZnO nanoparticles by Williamson–Hall and size–strain plot methods," Solid State Sci., vol. 13, no. 1, pp. 251–256, 2011, Doi:10.1016/j.solidstatesciences.2010.11.024.
[30] K. Roy, C. K. Sarkar, and C. K. Ghosh, "Green synthesis of silver nanoparticles using fruit extract

of Malus domestica and study of its antimicrobial activity," Dig. J. Nanomater. Biostruct, vol. 9, no. 3, pp. 1137–1147, 2014.
[31] R. I. Priyadharshini, G. Prasannaraj, N. Geetha, and P. Venkatachalam, "Microwave-mediated extracellular synthesis of metallic silver and zinc oxide nanoparticles using macro-algae (Gracilaria edulis) extracts and its anticancer activity against human PC3 cell lines," Appl. Biochem. Biotechnol., vol. 174, pp. 2777–2790, 2014.
[32] B. S. Saini and R. Kaur, "X-ray diffraction," Handbook of Modern Coating Technologies. Elsevier, pp. 85–141, 2021. Doi: 10.1016/b978-0-444-63239-5.00003-2.
[33] I. Jendrzejewska, R. Musioł, T. Goryczka, E. Pietrasik, J. Klimontko, and J. Jampilek, "The Usefulness of X-ray Diffraction and Thermal Analysis to Study Dietary Supplements Containing Iron," Molecules, vol. 27, no. 1, p. 197, Dec. 2021, Doi: 10.3390/molecules27010197.
[34] G. C. Dora, "Crystal structure analysis: a primer, by Jenny Pickworth Glusker and Kenneth N. Trueblood, 3rd edition, IUCr Texts on Crystallography, Vol. 14," Crystallogr. Rev., vol. 17, no. 2, pp. 157–160, 2011, Doi:10.1080/0889311x.2010.534988.
[35] Y. Meng, "A Sustainable Approach to Fabricating Ag Nanoparticles/PVA Hybrid Nanofiber and Its Catalytic Activity," Nanomater. (Basel, Switzerland), vol. 5, no. 2, pp. 1124–1135, Jun. 2015, Doi: 10.3390/nano5021124.
[36] P.-H. Chu et al., "Toward precision control of nanofiber orientation in conjugated polymer thin films: Impact on charge transport," Chem. Mater., vol. 28, no. 24, pp. 9099–9109, 2016.
[37] E. Baylan and O. A. Yildirim, "Highly efficient photocatalytic activity of stable manganese-doped zinc oxide (Mn: ZnO) nanofibers via electrospinning method," Mater. Sci. Semicond. Process., vol. 103, p. 104621, 2019.
[38] J. T. Mazumder et al., "First principle study on structural and optoelectronic properties and band-gap modulation in germanium incorporated tin (IV) oxide," Mater. Today Commun., vol. 27, p. 102393, 2021.
[39] P. Kumbhakar, C. Chowde Gowda, and C. S. Tiwary, "Advance optical properties and emerging applications of 2D materials," Front. Mater., vol. 8, p. 721514, 2021.
[40] A. Ashery, A. A. M. Farag, and M. A. Shenashen, "Optical absorption and dispersion analysis based on single-oscillator model of polypyrrole (PPy) thin film," Synth. Met., vol. 162, no. 15–16, pp. 1357–1363, 2012.
[41] H. A. Badran, H. F. Hussain, and K. I. Ajeel, "Nonlinear characterization of conducting polymer and electrical study for application as solar cells and its antibacterial activity," Optik (Stuttg)., vol. 127, no. 13, pp. 5301–5309, 2016.
[42] F. Yakuphanoglu, A. Cukurovali, and I. Yilmaz, "Single-oscillator model and determination of optical constants of some optical thin film materials," Phys. B Condens. Matter, vol. 353, no. 3–4, pp. 210–216, 2004.
[43] F. Yakuphanoglu, A. Cukurovali, and I. Yilmaz, "Determination and analysis of the dispersive optical constants of some organic thin films," Phys. B Condens. Matter, vol. 351, no. 1–2, pp. 53–58, 2004.
[44] D. Akinwande et al., "A review on mechanics and mechanical properties of 2D materials—Graphene and beyond," Extrem. Mech. Lett., vol. 13, pp. 42–77, 2017.

Journal of Basrah Researches (Sciences) **50**(2), 99 (2024)
DOI: https://doi.org/10.56714/bjrs.50.2.9

دراسة الخواص البصرية للبولي (3-هكسا ثايوفين -مشترك-ثايوفين ا) بنسب مختلفة للمونيمر

احمد اسماعيل عبدالله [1,*] ، حسين فالح حسين [1] ، صلاح شاكر اللعيبي [2]

[1] قسم الفيزياء، كلية التربية للعلوم الصرفة، جامعة البصرة، البصرة، العراق.

[2]قسم الكيمياء، كلية العلوم، جامعة البصرة، البصرة، العراق.

معلومات البحث

الاستلام 10 أيار 2024
المراجعة 8 اب 2024
القبول 15 اب 2024
النشر 31 كانون الأول 2024

الكلمات المفتاحية

بولي 3-هكسيل ثيوفين، بولي ثيوفين، البلمرة المشتركة، العلاقات بين البنية والملكية، الخصائص البصرية.

الملخص

تهدف هذه الدراسة الى تأثير نسبة البوليمر المشترك على الخصائص البصرية التي يمكن الاستفادة منها في تطبيقات الخلايا الشمسية. تم تحضير البوليمرات المشتركة بواسطة البلمرة المضافة. وتم تشخيص العينات حيث أظهرت نتائج الفحص بالأشعة السينية أن العينات المحضرة من البوليمرات النقية والمركبة تمتلك درجة عالية من التبلور. كما تميزت النماذج المذكورة أعلاه بطيف FT-IR، حيث أظهرت النتائج أن هذه الأغشية لها مجموعات فعالة واضحة. كما تمت دراسة الخصائص البصرية لجميع الأغشية المحضرة، مثل الامتصاصية ضمن المدى الطيفي (200 - 800 نانومتر) كدالة للطول الموجي، و فجوة الطاقة وطاقة التشتت وطاقة التذبذب الأحادي ومعامل الانكساروثابت العزل عند الترددات العالية ε∞، ومعاملات الزخم M-1 M-3، ، التأثرية البصريه من الدرجة الثالثة X3. بينت الدراسة أن طيف الامتصاص لأغشية المواد محل الدراسة يقع ضمن منطقة الطيف المرئي، حيث سجلت أعلى قمة للبوليمرات النقية والمشتركة عند الطول الموجي 485 – 495 نانومتر. بينت الدراسة أن فجوة الطاقة الضوئية لبوليمر P3HT (2.78 فولت) وللثيوفين (2.3 فولت) وتتناقص قيمة الفجوة مع زيادة معدل التطعيم حتى وصل إلى (1.88 فولت) عند معدل البوليمر المشترك 70% P3HT 30 %. وان سمك الغشاء متفاوتة تتراوح بين 49.1 إلى 10.2 نانومتر، وتراوحت الخشونة المسجلة لأسطح البوليمر من 20.7 نانومتر إلى 5.19 نانومتر..

Citation: A. Ismael et al., J. Basrah Res. (Sci.) **50**(2), 99 (2024).
DOI:https://doi.org/10.56714/bjrs. 50.2.9

***Corresponding author email :** ahmed.nano86@gmail.com

N: 1817-2695 (Print); 2411-524X (Online)
ine at: https://jou.jobrs.edu.iq